AD-A190 469 SUDDEN IONOSPHERIC DISTURBANCE MODEL UNCERTAINTY ASSESSMENT(U) NAVAL OCEAN SYSTEMS CENTER SAN DIEGO CA T N ROY ET AL. JUL 86 NOSC/TR-1140 1/1

UNCLASSIFIED F/G 4/1 NL

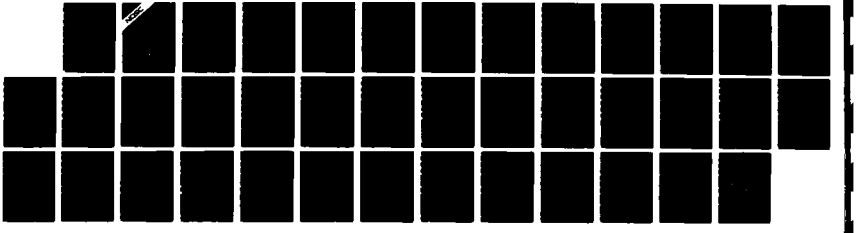

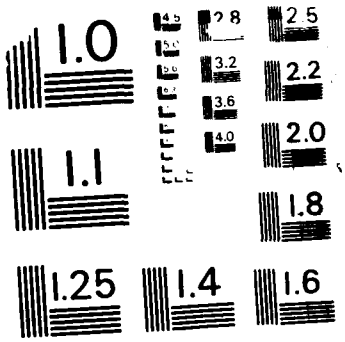

(4)

NOSC TR 1140

NAVAL OCEAN SYSTEMS CENTER San Diego, California 92152-5000

Technical Report 1140
July 1986

Sudden Ionospheric Disturbance Model Uncertainty Assessment

T. N. Roy
D. B. Sailors

NAVAL OCEAN SYSTEMS CENTER

San Diego, California 92152-5000

F. M. PESTORIUS, CAPT, USN
Commander

R. M. HILLYER
Technical Director

ADMINISTRATIVE INFORMATION

The work reported here was performed by members of the Ionospheric Branch, Ocean and Atmospheric Sciences Division, during the period October 1984–September 1986. The project was sponsored by the Space and Naval Warfare Systems Command. The authors wish to acknowledge three former members of the Ocean and Atmospheric Sciences Division, R.B. Rose, J.R. Hill, and M.P. Bleiweiss, for their original work in developing the SIDGRID model.

Released by
D.B. Sailors, Head
Ionospheric Branch

Under authority of
J.D. Richter, Head
Ocean and Atmospheric
Sciences Division

UNCLASSIFIED
SECURITY CLASSIFICATION OF THIS PAGE

REPORT DOCUMENTATION PAGE

A190 469

1a. REPORT SECURITY CLASSIFICATION UNCLASSIFIED	1b. RESTRICTIVE MARKINGS
2a. SECURITY CLASSIFICATION AUTHORITY	3. DISTRIBUTION/AVAILABILITY OF REPORT Approved for public release; distribution is unlimited.
2b. DECLASSIFICATION/DOWNGRADING SCHEDULE	
4. PERFORMING ORGANIZATION REPORT NUMBER(S) NOSC TR 1140	5. MONITORING ORGANIZATION REPORT NUMBER(S)
6a. NAME OF PERFORMING ORGANIZATION Naval Ocean Systems Center 6b. OFFICE SYMBOL (if applicable) Code 542	7a. NAME OF MONITORING ORGANIZATION
6c. ADDRESS (City, State and ZIP Code) San Diego, CA 92152-5000	7b. ADDRESS (City, State and ZIP Code)
8a. NAME OF FUNDING/SPONSORING ORGANIZATION Space and Naval Warfare Systems Command 8b. OFFICE SYMBOL (if applicable)	9. PROCUREMENT INSTRUMENT IDENTIFICATION NUMBER
8c. ADDRESS (City, State and ZIP Code) Washington, DC 20363-5100	10. SOURCE OF FUNDING NUMBERS PROGRAM ELEMENT NO: 31011G PROJECT NO.: RDDA TASK NO: 45BN AGENCY ACCESSION NO: DN288 591

11. TITLE (include Security Classification)

SUDDEN IONOSPHERIC DISTURBANCE MODEL UNCERTAINTY ASSESSMENT

12. PERSONAL AUTHOR(S)

T.N. Roy, D.B. Sailors

13a. TYPE OF REPORT	13b. TIME COVERED	14. DATE OF REPORT (Year, Month, Day)	15. PAGE COUNT
Final	FROM Oct 1984 TO Sep 1986	July 1986	39

16. SUPPLEMENTARY NOTATION

17. COSATI CODES			18. SUBJECT TERMS (Continue on reverse if necessary and identify by block number)
FIELD	GROUP	SUB-GROUP	HF propagation, computer prediction, sudden ionospheric disturbance (SID), Sudden Ionospheric Disturbance Model (SIDGRID), lowest obtainable frequency (LOF), lowest usable frequency (LUF), short-wave fade (SWF)

19. ABSTRACT (Continue on reverse if necessary and identify by block number)

The impact of a sudden ionospheric disturbance (SID) on HF propagation is discussed. The development of an empirically derived relationship (SIDGRID) to model this impact is presented. The SIDGRID model compared to 198 observed sounder data points. For distances less than 1500 km, the short-range prediction error was 0.5 MHz and in 95% of the tests the long-range prediction error was less than or equal to 2.0 MHz. Current FORTRAN and BASIC implementations of the model are given in Appendices C and D.

20. DISTRIBUTION/AVAILABILITY OF ABSTRACT	21. ABSTRACT SECURITY CLASSIFICATION	
☐ UNCLASSIFIED/UNLIMITED ☒ SAME AS RPT ☐ DTIC USERS	UNCLASSIFIED	
22a. NAME OF RESPONSIBLE INDIVIDUAL T.N. Roy	22b. TELEPHONE (include Area Code) (619) 553-3068	22c. OFFICE SYMBOL Code 542

DD FORM 1473, 84 JAN 83 APR EDITION MAY BE USED UNTIL EXHAUSTED
ALL OTHER EDITIONS ARE OBSOLETE

UNCLASSIFIED
SECURITY CLASSIFICATION OF THIS PAGE

EXECUTIVE SUMMARY

OBJECTIVE

Assess the accuracy of the Sudden Ionospheric Disturbance Model (SIDGRID) and present current computer implementations of the algorithm.

RESULTS

1. The NOSC solar X-ray/HF lowest observable frequency (LOF) algorithms provide an accurate assessment of the change in HF LOF for solar X-ray bursts greater than 1×10^{-3} erg/cm^2 $\times$ s and are valid over the entire sunlit hemisphere.
2. The SIDGRID model has the ability to display the disturbed lowest usable frequency (LUF) for any path on the geographical sunlit hemisphere at any date and time.
3. For distances less than 1500 km, the short-range prediction error was ± 0.5 MHz.
4. For distances greater than 1500 km, the long-range prediction error was less than or equal to ± 2.0 MHz in 95% of the tests.

RECOMMENDATIONS

1. Modify the SIDGRID model to include a means to adjust the resultant LUFs for system parameters such as transmitter power, antenna gains, required signal-to-noise ratio, and background radio noise.
2. Modify the SIDGRID model to improve the transition from disturbed to quiet time LUF prediction.
3. Develop the capability to calculate the D-region absorption arising from a short-wave fade (SWF).
4. Improve the model by eliminating the discontinuity at 1500 km, and make the model continuous as a function of range.
5. As the SIDGRID model has not been verified below an X-ray flux of 1×10^{-3} erg/cm^2 $\cdot$ s, it should be used with caution below this level.

CONTENTS

FIGURES

TABLES

1.0 INTRODUCTION

The effective operation of long-distance high-frequency (HF) communications systems has increased in proportion to the ability to predict variations in the ionosphere. These variations are affected in a complex manner by solar activity and seasonal and diurnal changes, as well as by latitude and longitude. Such a predictive capability has permitted communicators to optimize frequencies, antennas, and other circuit parameters.

Initially, manual methods were developed for analyzing ionospheric variations on HF circuits of short, intermediate, and long distances. Because the manual methods were laborious and time-consuming, various organizations developed computer programs to analyze HF circuit performance. A commonly predicted parameter in these programs is the maximum usable frequency (MUF). The MUF is the highest frequency that can be propagated by ionospheric refraction between points at a given time. Another commonly predicted parameter is the lowest usable frequency (LUF). The LUF is the lowest usable frequency propagated, and is determined by the amount of D-region absorption. The LUF over any circuit path is established as a function of total path absorption with respect to such HF system parameters as transmitted power, signal-to-noise ratio, and antenna gains.

More recently, the Naval Ocean Systems Center (NOSC) has developed a series of ionospheric prediction programs that will run on portable microcomputers. MINIMUF-3, MINIMUF-3.5, and MINIMUF-85 are examples of a series of NOSC-developed MUF models (ref 1–3).

This report will describe results of the uncertainty assessment of the SIDGRID model used to make LUF predictions for a disturbed ionosphere. The accuracy of both short-path and long-path predictions of the SIDGRID model will be discussed. The FORTRAN implementation of the SIDGRID model, routine DLOF, is listed in appendix C and the BASIC SIDGRID algorithm is listed in appendix D.

The SIDGRID model was compared to 198 observed sounder data points. Results from these tests indicate that the mean long-range prediction error was 0.24 MHz and the error between predicted and observed data was negligible in 29% of the tests. The probability that the prediction error was less than or equal to ± 1.0 MHz was 83% and the probability of error less than or equal to ± 2.0 MHz was 95%. For distances less than 1500 km, the short-range prediction error was ± 0.5 MHz.

2.0 COMMUNICATIONS DISTURBANCES CAUSED BY SOLAR FLARE ACTIVITY

2.1 DISTURBANCE PHENOMENA

Any system that is ionosphere-dependent is also dependent on solar activity and is subject to transient variations in solar radiation. There are two states of activity on the Sun that are of interest — the quiet state and the disturbed state. There are three broad categories of radiation that are of interest — X-ray, ultraviolet (UV), and particle emission. It is the abrupt change from the quiet to the disturbed state, which occurs during a flare on the Sun's surface, that causes a transient change in radiation levels and consequently causes abrupt changes in the Earth's ionosphere.

The quiet Sun radiates energy over nearly the entire electromagnetic spectrum. Each portion of the spectrum contributes to or affects the ionosphere in some way. Certain energy bands within each type of radiation provide the primary constituent for ionization at different levels within the Earth's atmosphere. This stratification creates distinct layers, which, together, form the ionosphere. The lowest, or D-region (50–90 km above the Earth), is believed to be formed by X-rays in the 1–10-Å spectrum and by Lyman α, UV, and particle radiation. The E-region (90–120 km) is created by X-rays in the 10–100-Å range and UV radiation between 100 and 1500 Å. The F-region (above 150 km) is formed by solar UV irradiation between 170 and 911 Å.

Solar flares are the source of most of the variable radiation that has important effects on the terrestrial and interplanetary environment. A solar flare is a localized chromospheric brightening on the sun and is sometimes accompanied by X-ray bursts, energetic nuclear particle emission, and radio frequency emissions. The size of the solar eruption will dictate the degree to which the various ionospheric regions are changed and the subsequent disruption of any ionosphere-dependent service.

During periods of solar disruption (flares, etc.), the energy levels of these three radiation forms abruptly change, which alters the structure of the ionosphere, changing the overall transfer function of the service propagating medium. These transient energy variations have wide and varying effects on ionosphere-dependent systems. There are two categories of disturbance phenomena: (1) short-term effects, which occur in close time correlation with the solar eruption and last for several hours after the event; and (2) long-term effects, which commence 24–36 hours after the event and last several days. Short-term effects are usually the result of enhanced X-ray, UV, and high-energy particle radiation, while long-term effects are caused by low-energy particle bombardment. Figure 1 shows the time event relationship of these phenomena.

The phenomena shown in figure 1 are summarized below (ref 4).

SHORT-WAVE FADE (SWF). A short-wave fade is a decrease or loss in signal strength of 3–32-MHz radio waves, caused by increased absorption due to 1–10-Å X-ray enhancement in the D-region and 10–100-Å X-ray enhancement in the lower E-region. Onset is in close coincidence with the solar eruption and the effects can last from several minutes to several hours, depending on the magnitude of the X-ray burst and the HF frequency of operation.

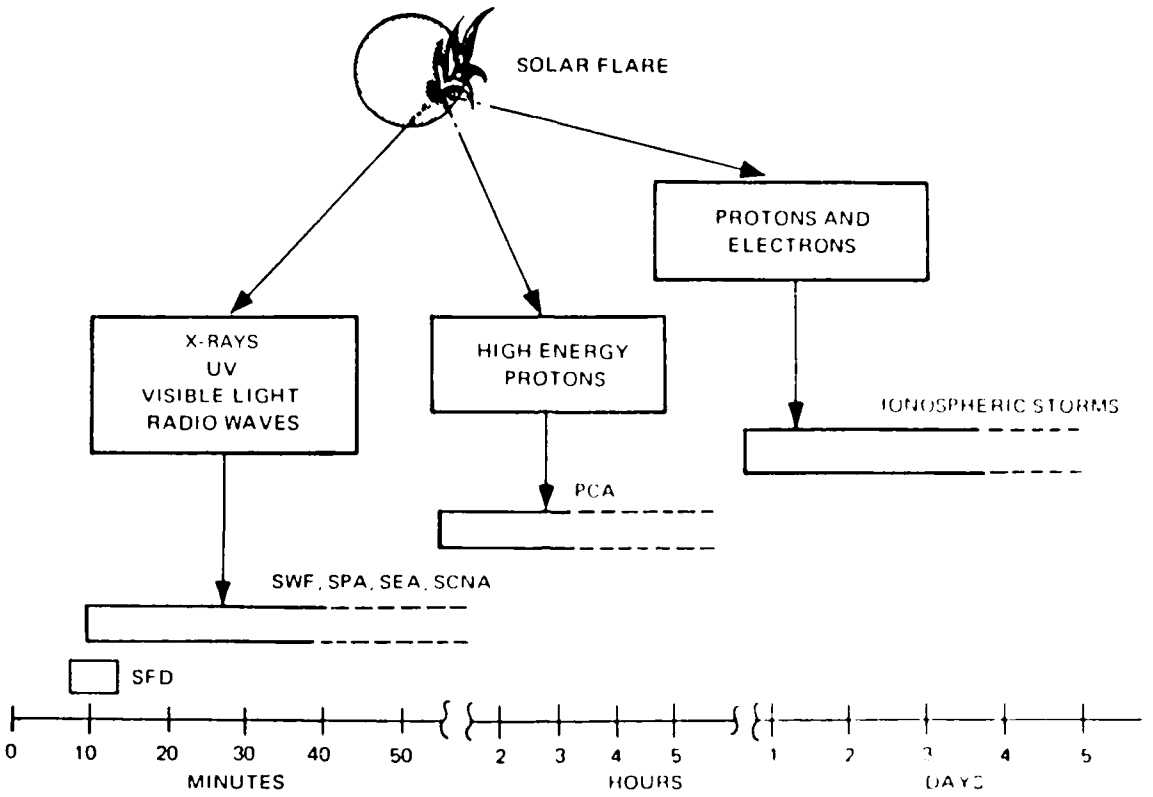

Figure 1. Disturbance phenomena (relative times)

SUDDEN PHASE ANOMALY (SPA). An SPA occurs when the ionization of the D-region is enhanced by 1–10-Å X-rays lowering the effective reflection height. This effect changes the phase of a sky-wave radio signal and is predominantly realized in the 3–30-kHz VLF frequency region. SPAs occur in close coincidence with the solar event, and effects can be noticed 1 to 2 minutes prior to, and concurrently with, the HF SWF.

SUDDEN ENHANCEMENT OF ATMOSPHERICS (SEA). SEA is another manifestation of D-region enhancement by solar X-rays and is denoted by an increase in low-frequency atmospheric noise in the VLF region (that is, thunderstorms at around 30 kHz).

SUDDEN COSMIC NOISE ABSORPTION (SCNA). The SCNA is a sudden decrease in signal strength of galactic cosmic noise received at frequencies high enough to penetrate the ionosphere, yet low enough to encounter measurable absorption. This phenomenon is characteristic of the 18–30-MHz frequency spectrum.

SUDDEN ENHANCEMENT OF SIGNAL (SES). An SES is a sudden increase in VLF signal strength caused by D-region enhanced ionization. Enhancement of the F-region by UV radiation is possible, although it is generally masked by D-region ionization.

SUDDEN FREQUENCY DEVIATION (SFD). An SFD is an impulse deviation in the frequency of 2–20-MHz radio waves reflected from the F-region of the ionosphere. This phenomenon is caused by ionization enhancements in the upper D-, E-, and F_1-regions caused by radiation above 100 Å and impulsive X-rays in the 4–20-Å wavelengths. It is characterized by a sharp peak deviation between 0.1 and 61 Hz (the average is approximately 1/2 Hz) and a decay back to zero deviation. The duration is approximately 15 minutes and is coincident with event onset.

SUDDEN IONOSPHERIC DISTURBANCE (SID). SID is a general term denoting the effects of enhanced ionization in the D-region and lower E-region by 1–10-Å X-rays over the entire sunlit hemisphere of the Earth. The SWF, SPA, SFD, SES, and SCNA are all different manifestations of the SID, depending on the portion of the ionosphere involved or the frequency of interest. SIDs are short-term disturbance phenomena occurring in close coincidence with the solar event.

IONOSPHERIC STORMS. The ionospheric storm is a long-term phenomenon resulting from a disruption of the Earth's magnetic field by particles (electrons and protons) ejected from a solar flare, and traveling at a speed of 1000-2000 km/min. The onset can be anywhere from 8 to 48 hours after a solar event and primarily affects the upper F-region. It is characterized by degraded HF radio propagation, high-latitude radio blackout, and sporadic E. The effects can last anywhere from 8 to 72 hours. At high latitudes, ionospheric storms create such phenomena as auroral displays and polar cap absorption (PCA) events.

POLAR CAP ABSORPTION (PCA). The PCA is a result of high-energy particle influx from a solar event and is evidenced by enhanced absorption of radio waves in the polar regions. The PCA starts from 1–4 hours after the solar event and can last from 1–3 days.

2.2 SWF FREQUENCY DEGRADATION

The characteristics of SWFs and their effects on HF systems have been discussed in references 5–8. For an HF user, the short-wave fade can produce short-term degradation that varies from minor signal loss to a total frequency blackout lasting up to several hours. The effects of the SWF are abrupt and in close time correlation with the actual solar event. Typically, the duration of the SWF is 1–4 hours. The mechanisms of a short-wave fade are reasonably well understood. Sky-wave propagation via the F-region passes through the lower D-region and is subject to absorption. During a solar disturbance, X-ray emissions irradiate the ionosphere, the depth of penetration depending on the spectrum of the X-ray flux, the solar zenith angle on the transmission path and the magnitude of the X-ray burst. If the penetration is of sufficient magnitude, the D-region ionization is enhanced, increasing absorption in this region of all signals passing through it. The immediate effect to the communicator is signal degradation or loss at the low end of the usable spectrum, and the LOF markedly increases 1 to 3 minutes after the onset of the event.

The SWF event is a daylight phenomenon, the intensity of which, on a given transmission path, depends on solar zenith angle and the peak magnitude and duration of the solar X-ray burst. The peak frequency penetration, or LOF increase, and the duration of the spectrum outage can be directly correlated to the shape and magnitude of 1–8-Å X-ray flux. The penetration of the LOF into the usable spectrum is a function of the magnitude of the X-ray burst and the solar position along the transmission path. A major event ($> 10^{-1}$ erg/cm^2 · s) will typically penetrate through about 3/4 of the usable spectrum. For a minor event (10^{-1} erg/cm^2 · s > X-ray flux > 10^{-2} erg/cm^2 · s), penetration will occur through half the usable spectrum.

In the HF spectrum, the D-region acts as a variable attenuator, with the total amount of absorption depending on (1) the number of times the signal passes through the D-region over a circuit path and (2) the launch angle of the signal. During daylight undisturbed conditions, the lower limit of the propagating spectrum [i.e., the lowest observed frequency (LOF)] is determined by the amount of D-region absorption. In the strictest sense, the LUF over any circuit path is also a function of such HF system parameters as transmitted power, signal-to-noise ratio, and antenna gain. For this reason, measured values of LOF will vary slightly for different paths and HF systems during undisturbed ionospheric conditions. When a solar flare occurs, the increased absorption in the D-region becomes the dominant factor in determining the LOF, causing it to rise. The amount it rises is proportional to the peak value of the X-ray enhancement and the solar zenith angle. A valid indicator of the impact of an SWF on a system's operation is the upward shift of the LOF.

For a given HF circuit, there exists a band of frequencies that will support propagation. The upper limit is bounded by the maximum observed frequency (MOF), which depends on the electron frequency of the E- or F-region, whichever is supporting propagation at that time. The lower boundary, called the lowest observed frequency (LOF), is controlled by the amount of nondeviative absorption in the ionospheric D-region. The band of frequencies between LOF and MOF is called the existing usable spectrum. The amount of absorption incurred as the signal passes through the D-region is controlled by solar radiation. As the sun rises, the electron density in the D-region increases, causing the HF absorption to increase proportionally to the inverse square of the propagating frequency. Therefore, during the day, absorption in the lower HF spectrum increases and the LOF rises as shown in figure 2a. The rise of the daylight LOF follows a secant solar zenith angle (χ) function.

During solar disturbances, the levels of solar X-rays rise, causing D-region absorption to increase. This has the effect of causing the LOF to rise proportionally to the increase in absorption. When the LOF meets the MOF, the circuit becomes completely blacked out. The phenomenon of the abnormal increase in LOF caused by the short-wave fade (SWF) is illustrated in figure 2b. Also shown is the 1-Å X-ray burst measured by the SOLRAD 9 satellite. The close correlation between changes in the HF LOF and 1–8-Å X-ray flux can be easily seen.

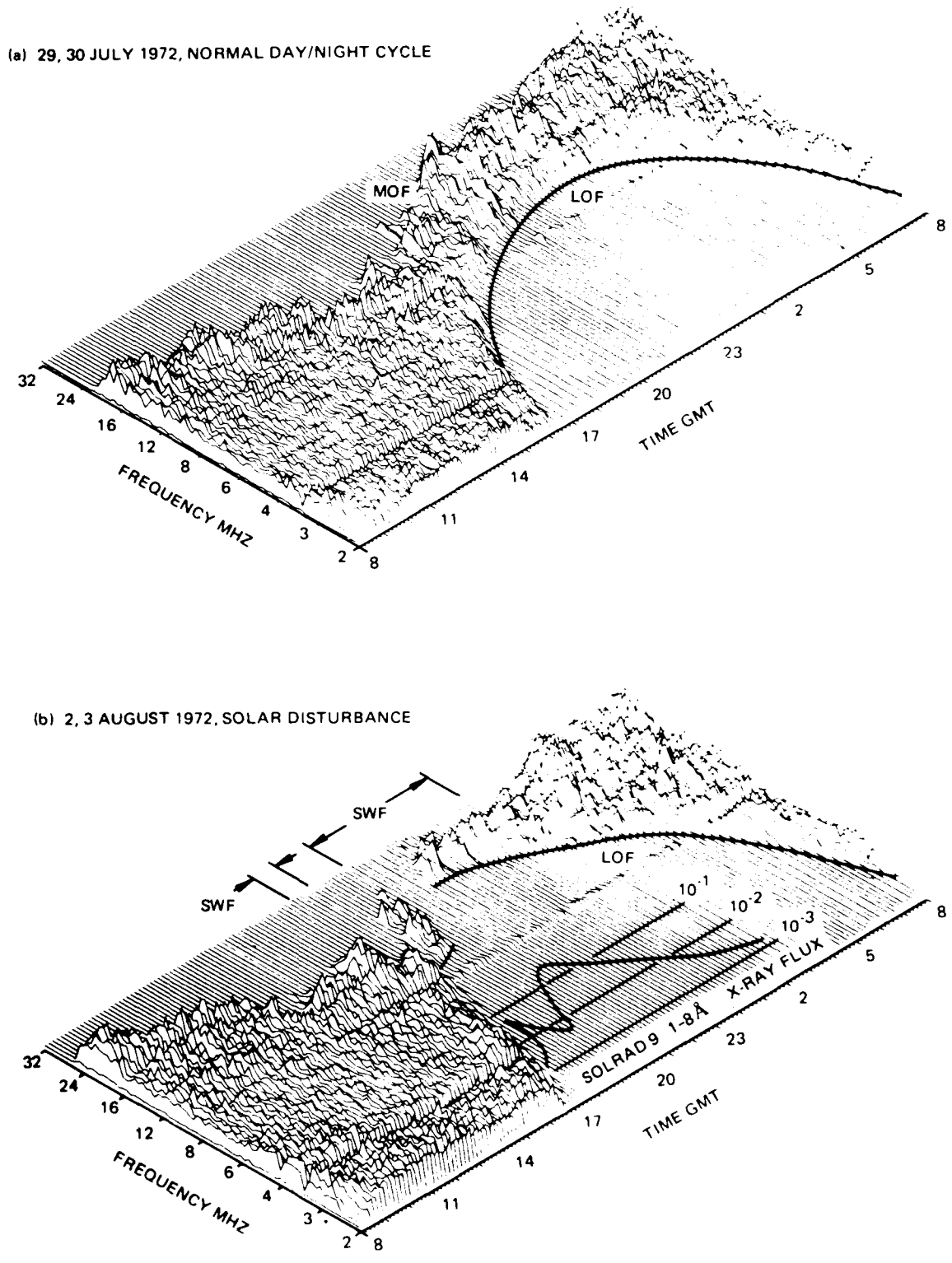

Figure 2. 24-hour HF propagation characteristics, Guam to Hawaii. Time resolution: 1 line = 10 min avg. Signal amplitude: $\chi = 25$ dB above receiver threshold.

The solar zenith angle is one of the major factors in determining the degree to which ionization takes place in the lower atmosphere. The increase in angle of incidence of the solar radiation imposes a greater path length for a given penetration of the X-ray flux into the ionosphere. A propagation path with reflection points near the terminator (day-night transition) will exhibit much less signal absorption during a solar X-ray event than will a similar path with reflection points near the subsolar location. This is because the X-ray flux penetrating near the terminator must pass through considerably more ionosphere (because of the steep angle of incidence) before reaching the D-region where the HF absorbing ionization must be generated. A large portion of the X-ray energy is therefore lost before reaching the D-region. At the subsolar point, the shortest path to the D-region is present and the greatest quantity of X-ray penetration is achieved.

3.0 SUDDEN IONOSPHERIC DISTURBANCE MODEL (SIDGRID)

SIDGRID is an extension of the development of a simple LOF model that could be varied as a function of real-time solar X-ray flux measurements during solar flares. This model was the first truly real-time, sudden ionospheric disturbance (SID) assessment capability for a system like PROPHET (ref 9). The close correlation between the concurrent rise in solar 1-Å X-ray flux and HF LOF led to the development of a simple first-order algorithm relating the two as a function of solar zenith angle.

During development of the algorithm, it became evident that variation in the LOF versus X-ray flux dependency on transmission path length was such that a single, range-independent model would not satisfy all requirements. Analysis showed that improved results could be obtained if the transmission paths were separated into two categories – short-range for anything less than 1500 km and long-range for everything greater. Two different algorithms were developed, one for each range category. A brief theoretical discussion of the formulae used to derive the algorithms is given in appendix A.

3.1 METHOD OF CALCULATION

The long-range LUF X-ray flux model is an empirically derived relationship. The first step was to plot the 1-8-Å X-ray flux, as measured by the SOLRAD 9 satellite, versus the LOF during the onset of two SWFs observed over the Hawaii-to-California oblique sounder path on 30 and 31 October 1968. These two events were chosen because of similar rise and peak characteristics of the 1-8-Å flux, as shown in figure 3. The difference in LOF noted between the two curves arises from the different solar zenith angle (χ) when the events occurred. The next step was to derive a function to account for χ. By "trial and error" techniques, the LOF at a given time was multiplied by a factor of ($1.0 + \sec^2\chi$ 10), which moved the curves together. By curve-fitting techniques, the relationship between true LUF corrected for zenith angle (F') and the 1-8-Å X-ray flux was determined, to a first order of approximation, to be:

$$\text{Flux}(1\text{-}8\text{-Å}) = (0.01038)(F' - 15).$$

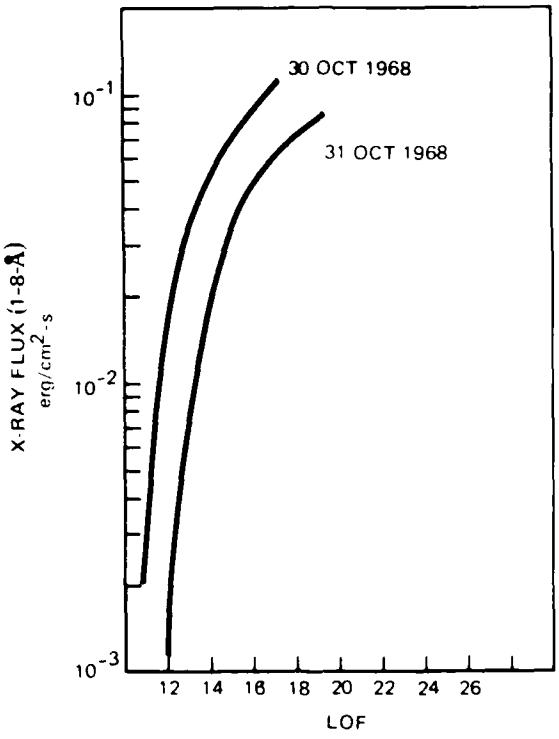

Figure 3. X-ray flux vs HF LOF.

Further investigation expanded this equation to provide a better fit, the final equation being:

$$\text{Flux} - 0.01038\,(f_1 - 15.0) + 0.003 \sin\left[0.8491\,(f_1 - 15.6)\right] = 0 \qquad (1)$$

where

$$f_1 = \text{LOF}\left[\frac{1 + \sec^2 \chi}{10}\right] . \qquad (2)$$

To find the LUF, equations (1) and (2) are solved by Newton's method, using the given values of χ and LUF. Newton's method refines an initial guess x_0 of a solution of a general nonlinear equation $f(x) = 0$. It takes the following form:

$$x_{i+1} = x_i - \frac{f(x_i)}{\frac{\partial}{\partial x} f(x)} \quad (i = 0, 1, 2, \ldots) \qquad (3)$$

where $x_0 = (\text{Flux} \cdot 0.1038 + 150)\ (10 + \sec^2 \chi)$.

In equation (1), $x = \text{LUF}$. To use Newton's method, we evaluate $\partial/\partial x\ f(x)$ and get:

$$\frac{\partial}{\partial x} f(x) = \frac{f_1 \left\{0.01038 - 0.0025473 \cos\left[0.8491\,(f_1 - 15.6)\right]\right\}}{\text{LUF}} . \qquad (4)$$

To find the subsolar point, the Greenwich hour angle (GHA) and solar declination are used. The solar zenith angle (χ) is computed from

$$\chi = \cos^{-1} |\sin(\alpha) \sin(\delta) + \cos(\alpha) \cos(\delta) \cos(\gamma - \beta)| \quad (5)$$

where

α = latitude of grid point
β = longitude of grid point
δ = latitude of subsolar point = declination
γ = longitude of subsolar point = 15 GHA.

The short-range algorithm was developed by the same techniques discussed above for the long-range algorithm, but with a different data set. An extensive search did produce a period in 1971 when oblique sounder strip chart recordings were made of the now-defunct Davis, California, sounding transmitter. Enough information was assembled to derive the desired algorithm.

Davis to La Posta, California, is an 803-km, north-to-south path. Between 2 July and 20 November 1970, 10 HF SWF disturbances were recorded. Table 1 identifies the disturbances analyzed.

Table 1. 1971 SWF disturbances – Davis to La Posta, CA.

Event	Date	Time	1-8-Å X-ray Peak*
1	2 Jul 1971	1845	2.2×10^{-2} erg/cm^2 · s
2	7 Jul 1971	1507	6.3×10^{-3} erg/cm^2 · s
3	7 Jul 1971	1603	8.9×10^{-3} erg/cm^2 · s
4	7 Jul 1971	1925	2.8×10^{-3} erg/cm^2 · s
5	7 Jul 1971	1947	5.3×10^{-3} erg/cm^2 · s
6	10 Jul 1971	1546	1.3×10^{-2} erg/cm^2 · s
7	12 Sep 1971	1624	4.4×10^{-2} erg/cm^2 · s
8	10 Nov 1971	0000	4×10^{-2} erg/cm^2 · s
9	12 Nov 1971	1833	2×10^{-2} erg/cm^2 · s
10	20 Nov 1971	2049	1.8×10^{-2} erg/cm^2 · s

*Derived from SOLRAD 9 satellite 1-8-Å X-ray data.

The new algorithm was tested against all available short-range SWF data, and it became obvious that the basic SIDGRID model would require modification to provide the dual-algorithm capability. On completion of the necessary modifications, the over-all concept was tested by use of an SWF disturbance that was measured simultaneously over long-range and short-range paths. Event 8 in table 1 is such an event.

From theoretical considerations, the form of the formula can be given by

$$F^n = aF_x \cos^m \psi, \quad (6)$$

where

F = LUF (MHz)
ψ = solar zenith angle
F_x = X-ray flux.

The contributions of energy other than solar X-rays are assumed to be a constant effect. The values of n, m, and a are to be found by use of the observations. A theoretical value for n can be found by noting the following simplified model for absorption. Electron production rates, q, in the D-region of the ionosphere can be given by

$$q = c_1 F_x \cos^m \psi, \tag{7}$$

and q is related to the electron density at equilibrium by

$$q = \alpha N^2. \tag{8}$$

The absorption at a point in the ionosphere at which the electron collision frequency is ν can be calculated from

$$A = c_2 N \nu / f^2. \tag{9}$$

It is assumed that total absorption is proportional to some weighted average electron density, N, which is related to the 1-Å flux by equation 8. By combining equations 6–9, it is found that

$$A^2 = cF_x \cos^m \psi f^{-4}, \tag{10}$$

where A is an absorption cutoff level determined by noise and signal-processing considerations. The value of $n = 4$ has been found to fit the data quite well. To find m, we reduce equation 6 to a linear equation in $\cos^m \psi$ by taking logarithms

$$\ln (f_x f^4) = m \cdot \ln (\cos \psi) + \ln (a). \tag{11}$$

Solving for a and m, we obtain a formula of the form of equation 10, in which the constant 1.0191×10^{-3} is the absorption cutoff level:

$$(1.091 \times 10^{-3})^2 = f^{-4} (F_x \cos^3 \psi). \tag{12}$$

It was found that when 1-8Å X-ray flux was below 1.85×10^{-3} erg/cm^2 · s, a "quiet" or undisturbed approximation could be used:

$$f^4 = 1785 \cos^3 \psi. \tag{13}$$

This formula was derived from pre-event undisturbed data shown in table 2.

3.2 DESCRIPTION OF DATABASE

The long-range algorithm was derived by using data from two SWF events over two HF transmission paths. To ascertain how valid this algorithm is for other paths and different times and seasons, the following four-step process was performed.

Step 1. From the NOSC La Posta historical data files of HF oblique sounder data, HF short-wave fades were selected for the period between 1969 and 1972. Two types of SWF disturbance data were chosen: (1) multiple SWFs observed over a single transmission path in the same 24-hour period; and (2) a single or double SWF event observed over more than one path in the same 24-hour period. At this stage, only the facts that an SWF was evident on the HF sounder recorder and that the data were suitable for further analysis were noted. No frequency/time data were recorded at this time.

Step 2. Once the date and time of an SWF was chosen, a 1-8-Å X-ray flux versus time plot for the same period was prepared from the NRL SOLRAD 9 satellite solar radiation records.

Step 3. After the 1-8-Å X-ray flux levels were known as a function of time, the proper LOF paths were selected and the HF transmissions were plotted. Under the assumption that the highest LOF indicated along the plotted HF path will control the overall path LOF, a plot of predicted LUF versus time was prepared.

Step 4. Once the predicted LUF/time plot was completed, the HF sounder records were analyzed and the observed LOF versus time was plotted for the same events. In this manner, the SIDGRID model was tested in a quasipredictive mode, with only time and X-ray flux levels being used to vary output, and then compared to actual observations. Care was exercised not to influence predicted LUF deviations with prior knowledge of the actual event.

Table 2 summarizes the X-ray disturbances selected for this test. A total of 26 events between 4 November 1968 and 7 August 1972 were used. In the classification of X-ray bursts, it has been found that only bursts whose 1-8-Å flux level rises above 1×10^{-2} erg/cm^2 · s produce appreciable SWFs on HF circuits. This test is concerned with two classes of bursts: small bursts or Class M ($1 \times 10^{-2} <$ flux $< 1 \cdot 10^{-1}$), and moderate to large bursts or class X ($1 \times 10^{-1} <$ flux). A burst that peaked at 5×10^{-2} erg/cm^2 · s would be denoted as an M5 event. Of the 26 events, 14 were Class M and 12 were Class X. The durations of the X-ray bursts ranged between 15 and 330 minutes. There is an excellent cross section of characteristics included, ranging from very sharp impulsive changes to very slowly changing bursts. The smallest burst tested was an M2 and the largest was an X4. A complete cross section of solar zenith angles is represented in the data sample, ranging from the midday case (0) to the sunrise and sunset case, for which χ is close to 90 . When the same event is tested on several paths, the effects of different solar zenith angles can be compared.

Table 2. Summary of events tested.

Event	Date	Start Time	Size of 1-8-Å X-ray Burst	Duration of SWF, min	Number of HF Paths Tested	Solar Sunspot Number
1	4 Nov 1969	0400	X2	40	1	105
2	11 Nov 1969	0030	M2	40	1	105
3	11 Nov 1969	0130	M7	90	1	105
4	11 Nov 1969	0400	X1	40	1	105
5	11 Nov 1969	0450	M5	30	1	105
6	11 Nov 1969	0520	X1	90	1	105
7	11 Nov 1969	0710	M5	15	1	105
8	11 Nov 1969	0810	X3	30	1	105
9	27 Nov 1969	0030	M3	330	1	105
10	22 Jul 1970	0010	X2	60	3	103
11	12 Aug 1970	2000	X3	120	3	101
12	16 Nov 1970	0030	X2	90	2	89
13	16 Nov 1970	2120	M4	40	2	89
14	16 Nov 1970	2220	M5	60	2	89
15	17 Nov 1970	0110	M5	50	2	89
16	17 Nov 1970	1740	X1	40	2	89
17	17 Nov 1970	2010	M5	30	2	89
18	17 Nov 1970	2120	M2	20	2	89
19	17 Nov 1970	2220	M5	40	2	89
20	18 Nov 1970	0140	X2	50	2	89
21	2 Aug 1972	0310	X2	120	2	65
22	2 Aug 1972	1810	M5	70	2	65
23	2 Aug 1972	2000	X3	240	2	65
24	4 Aug 1972	0620	X4	120	4	65
25	7 Aug 1972	0200	M3	90	4	65
26	7 Aug 1972	0340	M5	70	4	65

Table 3 lists the HF sounder paths where data were recorded during the events listed in table 2. Data from light transmission paths were tested, spanning the Pacific area from California to Northwest Cape, Australia. Here, again, a variety of transmission path characteristics are represented.

Table 3. Summary of HF transmission paths tested.

Path	Path Length km	Path Latitude	Events Tested (From Table 2)
COMMSTA Honolulu, Hawaii, to Southern California	4100	W-E midlat	10,11,12,13,14, 15,16,17,18,19, 20,21,22,23
Davis, California, to COMMSTA Kodiak, Alaska	3100	S-N midlat	10,11
COMMSTA Honolulu, Hawaii, to COMMSTA Kodiak, Alaska	4100	S-N midlat	12,13,14,15,16, 17,18,19,20
COMMSTA Guam to COMMSTA Honolulu, Hawaii	6000	W-E low midlat	10,11,21,22,23, 24,25,26
COMMSTA Guam to COMMSTA HEH, Australia	5300	N-S transequatorial	2,3,4,5,6,7,8, 9,24,25,26
COMMSTA Guam to COMMSTA Japan	2700	S-N low midlat	24,25,26
COMMSTA Philippines to COMMSTA Japan	3000	S-N midlat	No tests performed
COMMSTA Philippines to COMMSTA HEH, Australia	4300	N-S transequatorial	1
COMMSTA Honolulu, Hawaii, to COMMSTA Japan	6000	E-W midlat	24,25,26

3.3 DISCUSSION OF ACCURACY STUDIES

3.3.1 Long-Range Algorithm Tests

Figure 4 is a series of graphs (a–t) showing predicted LUF (solid lines) and observed LOF (dashed lines) versus time for the 26 SWF events resulting from the solar X-ray bursts listed in table 3. Each point plotted in these graphs represents one test of the SIDGRID model.

Figures 4 a, b, and c show three different SWF situations: a short, impulsive event caused by an X2 X-ray burst with very steep rise and decay (a); a very slow, long-lasting M3 event (b); and a series of seven Class M and X events occurring in a 9-hour period (c). Of interest is the fact that these events occurred in 1969, near the peak of the solar cycle, and the transmission paths tested are markedly different from the path that was used to derive the original LUF/X-ray flux algorithm. A total of 38 points were tested on this path, with the error exceeding ±1 MHz in only one case.

Figures 4 d and e depict two Class X events in 1970. In each event, data from three different Eastern Pacific (EASTPAC) HF transmission paths were plotted. Errors between predicted and observed LOF variations occur in the decay portion of the event. In figure 4 d, the greatest error observed was on the Hawaii-to-California path between 0100 and 0200 UT, where the predicted LUF is 1.5 MHz below observed data. The

same trend appears in figure 4 for the same path. However, in figure 4e for the California-to-Kodiak, Alaska, path the trend is reversed and the predicted LUF is 1.5–2.0 MHz higher than the observed LOF.

Figures 4f and g contrast the effects of a large X2 event and a pair of small Class M events, which occurred 16 November 1970. Figure 4f shows the Hawaii-to-California path (W-E) and the Hawaii-to-Kodiak, Alaska, path (S-N). The decay portion of the predicted X3 SWF follows exactly the observed data on both paths. On the M4 and M5 SWFs, some error is evident and results from a lack of frequency resolution in sounder data and also from a variation in frequency characteristics of the predicted LUF algorithm at the lower flux level. In all cases, the error is less than 2 MHz and, more typically, it is 0.5 MHz.

Figures 4h and i depict another multiple SWF event period, which occurred 17 and 18 November 1970. Again, two paths are shown: Hawaii-to-California and Hawaii-to-Alaska events. These figures illustrate the different impact of the same SWF on different transmission paths, depending on path illumination. At 0130 UT, both paths are still sunlit, and the M5 X-ray burst produces about the same effect. At 1800 UT, the Hawaii-to-California path has just finished sunrise, while the Hawaii-to-Kodiak, Alaska, path is still dark. The X1 event produces a significant SWF on the sunlit path and no effect on the darker path. The SIDGRID model accurately predicted the impact. Throughout the remaining daylight hours, three additional Class M events produced minor SWFs and comparisons show good correlation between predicted and observed results. Between 0000 UT and 0200 UT on 18 November, the observed LOF drops below the predicted LUF on both paths. It should be noted that the observed LOF is anomalously low for this time of day when compared to normal daytime LOF trends. In addition, through this period, the 1–8-Å X-ray flux never dropped below 5×10^{-3} erg/cm^2 · s, which should have tended to keep the LOF at or slightly above undisturbed levels. The final event occurred during sunset transition at 0230 UT, and again the model accurately predicted the SWF variations over the two paths. Except for the one inconsistent period between 0000 and 0200 UT, predicted LUFs correlated to observed LOFs during a sunrise transition, a sunset transition, and peak daylight hours. This demonstrates the model's capability to assess SWF impact over a large geographical area.

The test would not be complete without a review of some of the SWF events that occurred in August 1972. The period between 2 and 10 August 1972 was the most sustained period of solar/ionospheric disturbances during this solar cycle. Figures 4j and k show three SWF disturbances on 2 August on the east-west paths between Hawaii and California, and between Guam and Hawaii. The first X2 event at 0400 UT shows again the different SID impact as a function of path longitude. Between Hawaii and California, the sun has almost set and the impact of this flare is minor. However, the Guam-to-Hawaii path is still completely illuminated, and the frequency fadeout over this path approaches 31 MHz. At 1900 UT, over this same path, the M5 X-ray burst tends to accelerate the sunrise increase in LOF, while on the Hawaii-to-California path, the M5 event products a minor SWF. At 2030 UT, the X3 event produces total fadeout over both paths, which are now totally illuminated. The display used in the analysis of these two events is included in appendix B for reference.

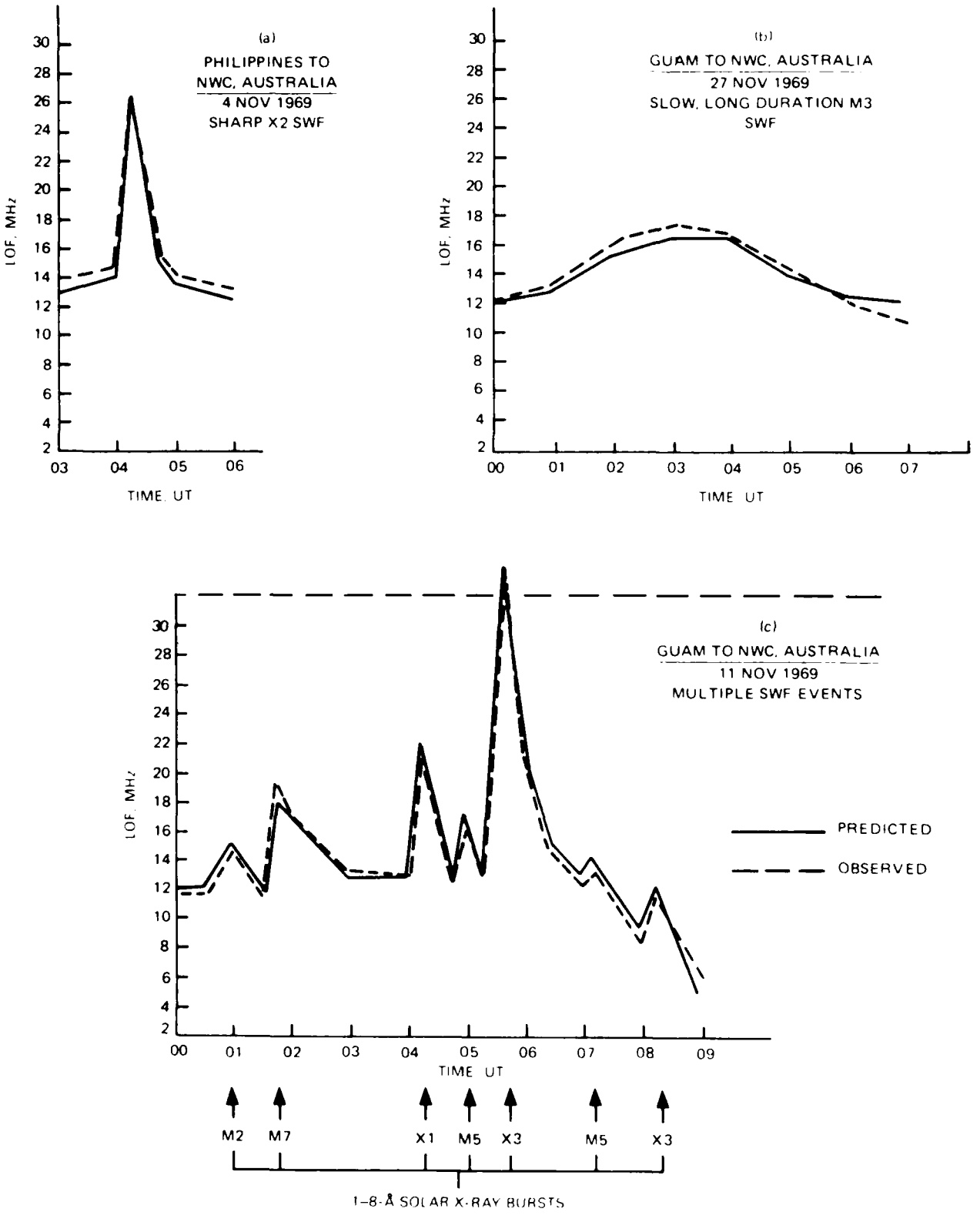

Figure 4. Comparison of predicted and observed HF SWFs

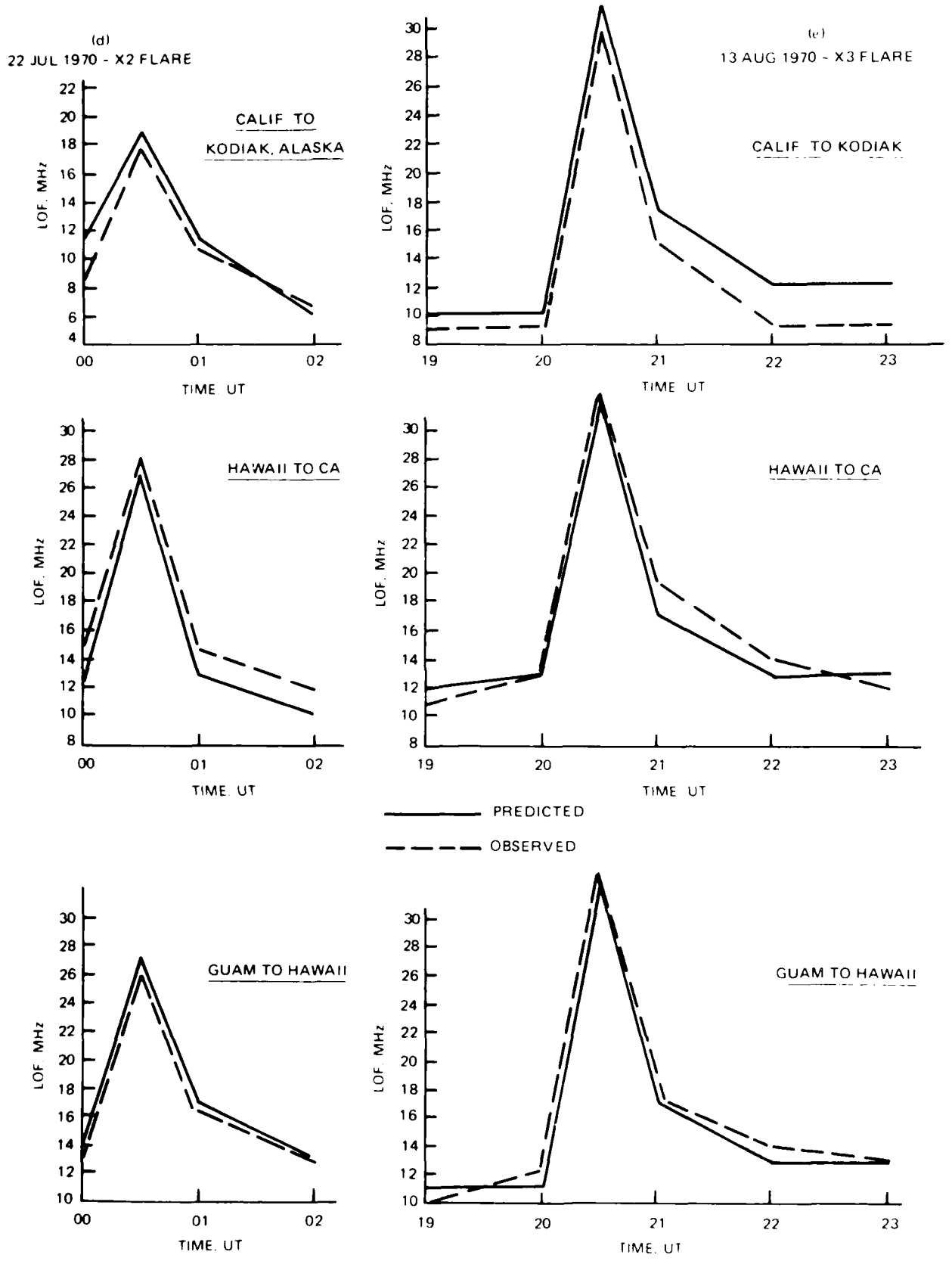

Figure 4. (Continued).

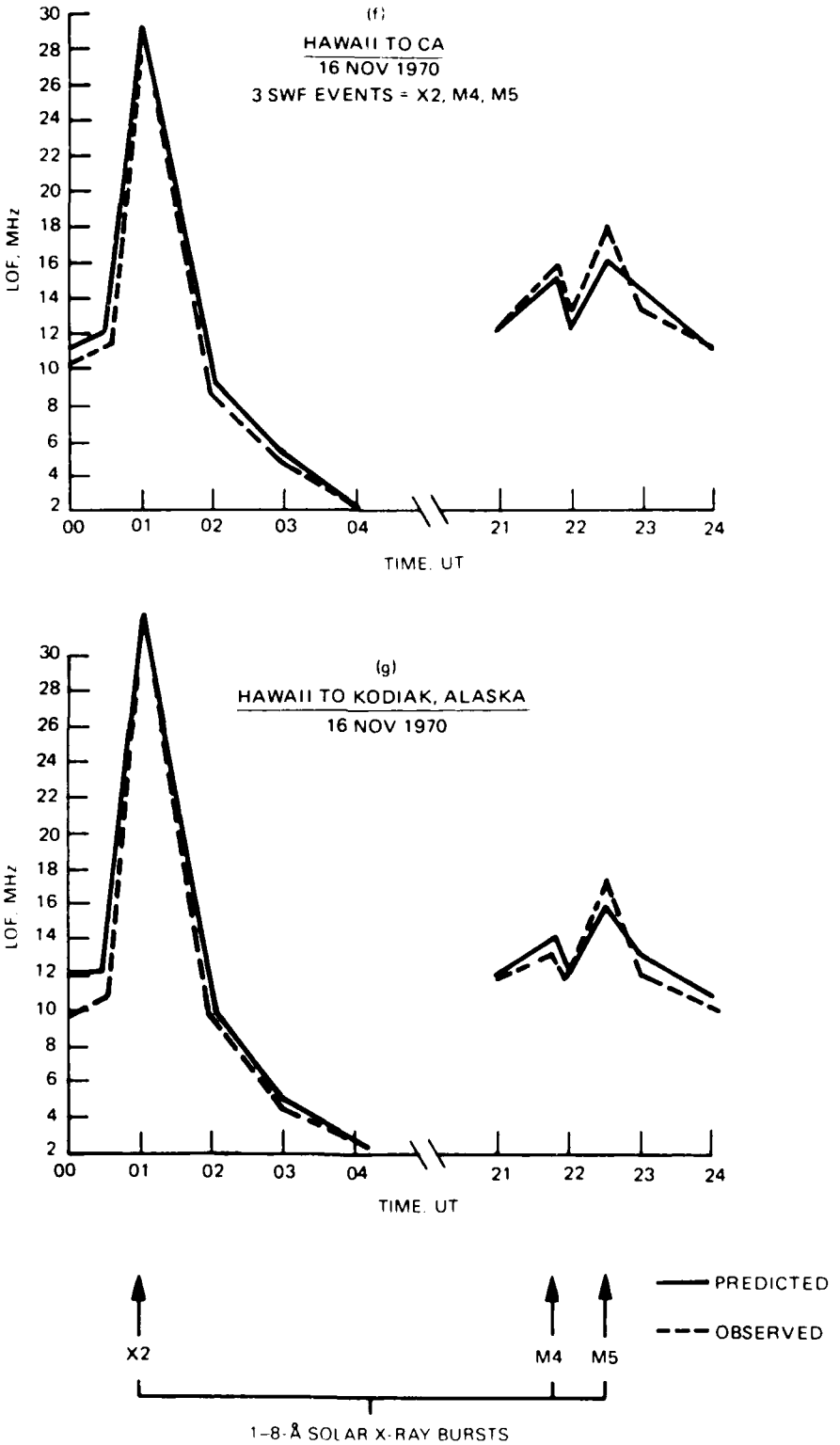

Figure 4. (Continued).

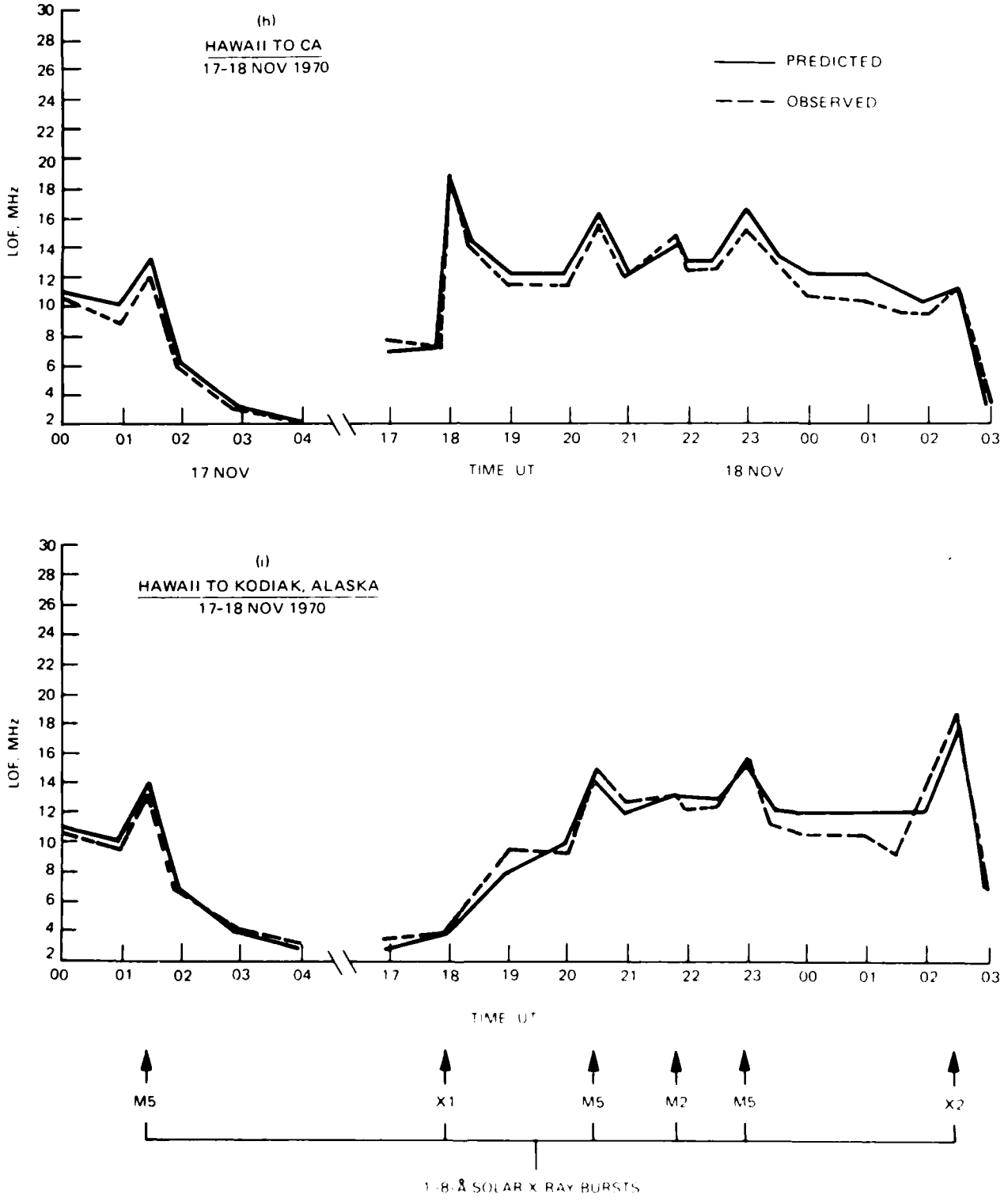

Figure 4 (Continued)

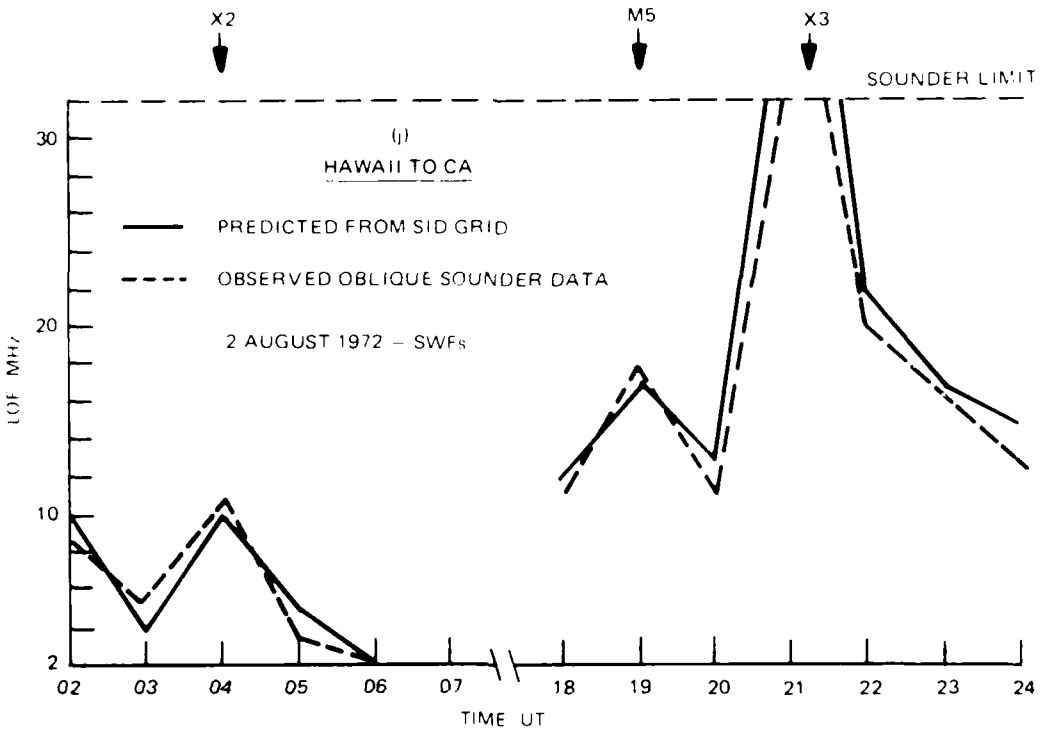

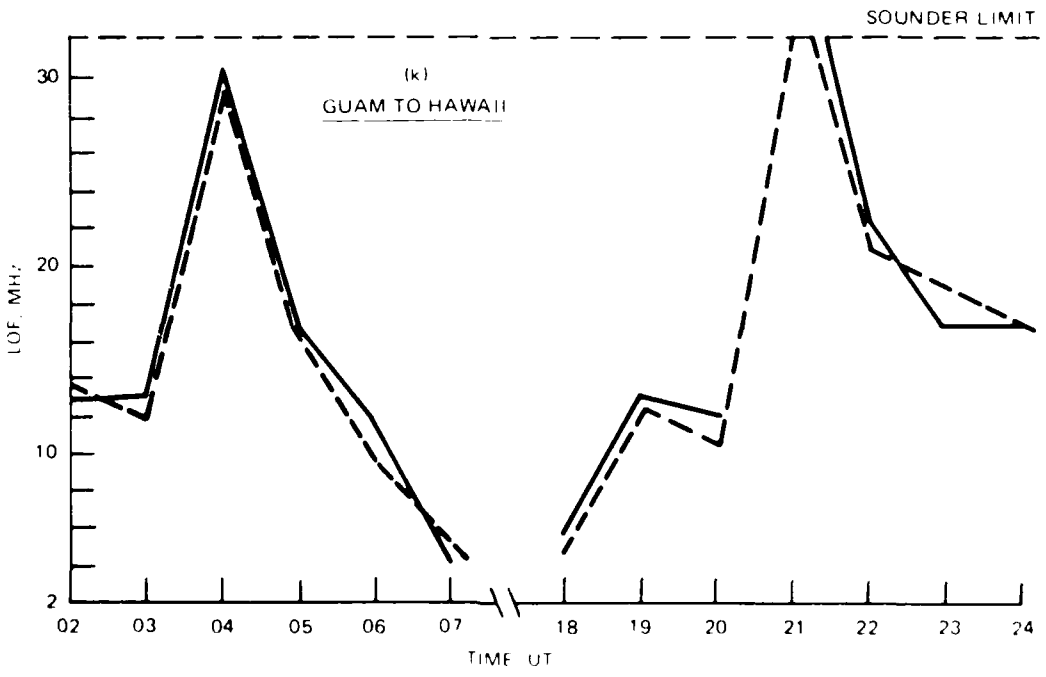

Figure 4. (Continued).

Figures 4 l −o show the effect of the X4 X-ray event of 4 August on four Pacific paths. Note the difference in impact over these paths. The outage time at 18 MHz varies between 30 and 90 minutes, and the model was able to accurately predict these variations over the four paths.

Figures 4 p−t show a pair of small Class M events on 7 August, again for four Pacific paths. While the Guam-to-Hawaii and Guam-to-Japan paths correlate accurately, the Guam-to-Japan and Hawaii-to-Japan predictions show a consistently higher predicted LUF than observed. Of all the SWF events and transmission paths tested, the plots in figures 4 s and t show the poorest correlation. There is one possible reason for this error. First, HF sounder data received from Japan show a high daytime noise environment, making changes in LOF difficult to interpret. Once the observed LOF rises above 16 MHz, the noise contamination no longer is a problem. The large X4 event of figure 4 m shows an accurate comparison between predicted and observed values, while the smaller M3 and M5 events of figures 4 s and t involve LOF variations between 10 and 16 MHz, the part of the spectrum most degraded by the local noise environment.

Overall, 198 data-point tests were made, comparing SIDGRID predictions to observed sounder data. From these tests it was determined that:

1. The mean prediction error is 0.24 MHz high.
2. The error between and observed data was negligible in 29% of the tests.
3. The probability that prediction error $\leqq \pm 0.5$ MHz = 48%.
4. The probability that prediction error $\leqq \pm 1.0$ MHz = 83%.
5. The probability that prediction error $\leqq \pm 2.0$ MHz = 95%.

The cross-sectional data tested indicate that the model can produce valid predictions for the entire sunlit hemisphere, given date, time, and X-ray flux. An accuracy specification of ± 2.0 MHz is valid for X-ray flux levels down to 10^{-3} erg/cm^2 · s, an essentially undisturbed condition. For X-ray fluxes of 5×10^{-2} or greater, the ± 0.5-MHz error specification is more appropriate. When the initial LUF/X-ray flux algorithm was developed, it was stipulated that it was for a disturbance case and probably not valid for quiet solar conditions when the X-ray flux is between 10^{-4} and 10^{-3}. However, these tests show that the SIDGRID model produces usable results even at these low flux levels.

3.3.2 Short-Range Algorithm Tests

The first performed test of the short-range disturbance algorithm used the SWF disturbances listed in table 1. The same testing procedures outlined above were again followed. Table 4 summarizes the results of the initial tests. From the nine events tested, the calculated SWF/LUF varied from the observed SWF over a range of −0.54 MHz to +0.20 MHz. The largest deviation occurred in the 12 November 1971 event, where it should be pointed out that the peak X-ray flux was approximated, since sensor saturation occurred. Also, in the frequency between 2 and 4 MHz, the resolution of the UPR-2 sounding receiver is 0.1 MHz. Between 4 and 8 MHz, the resolution is 0.2 MHz. If these limitations on the data are taken into account, it is felt that a nominal accuracy specification for the short-range algorithm is ± 0.5 MHz for HF transmission paths of less than 1500 km.

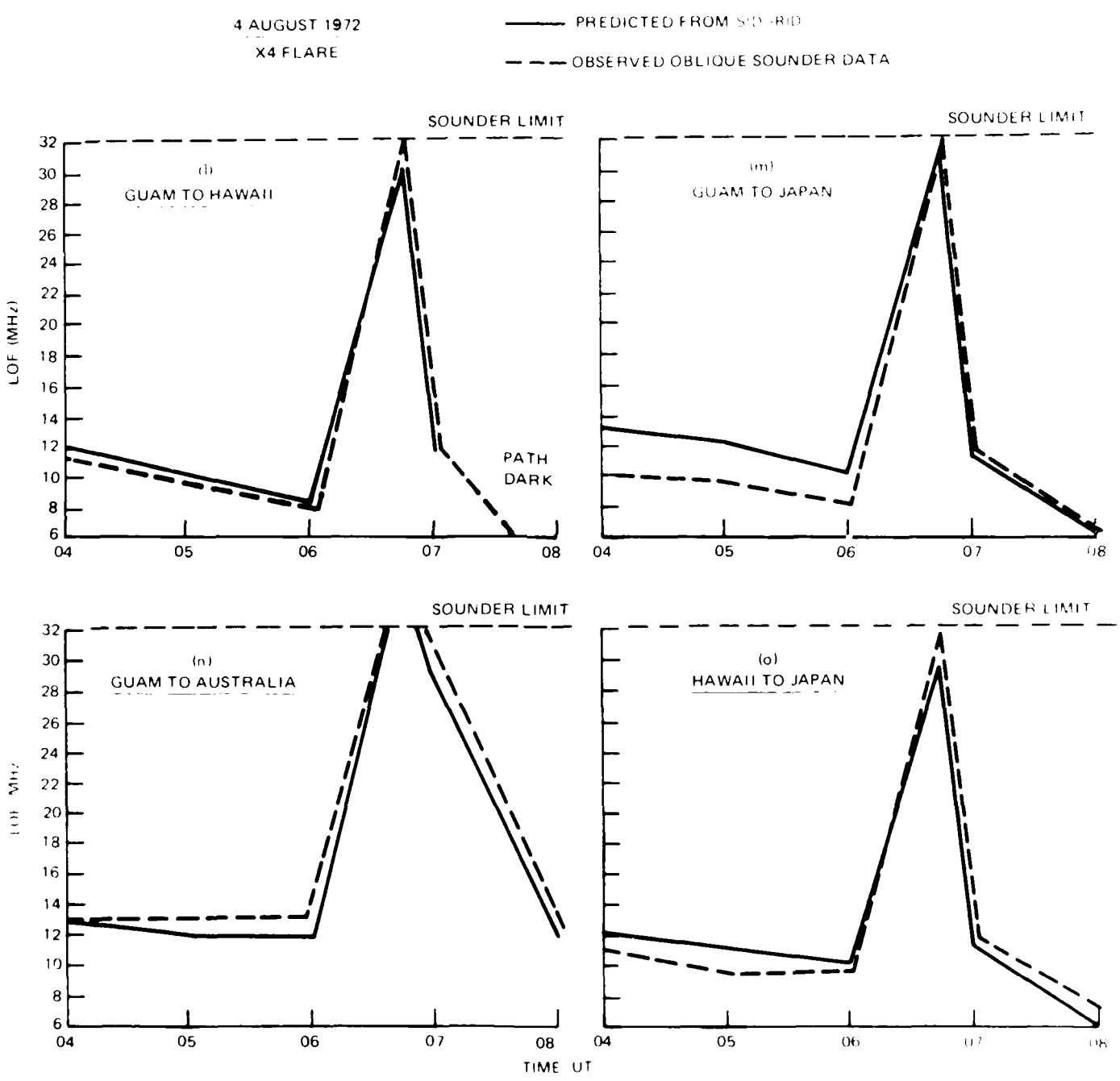

Figure 4. (Continued)

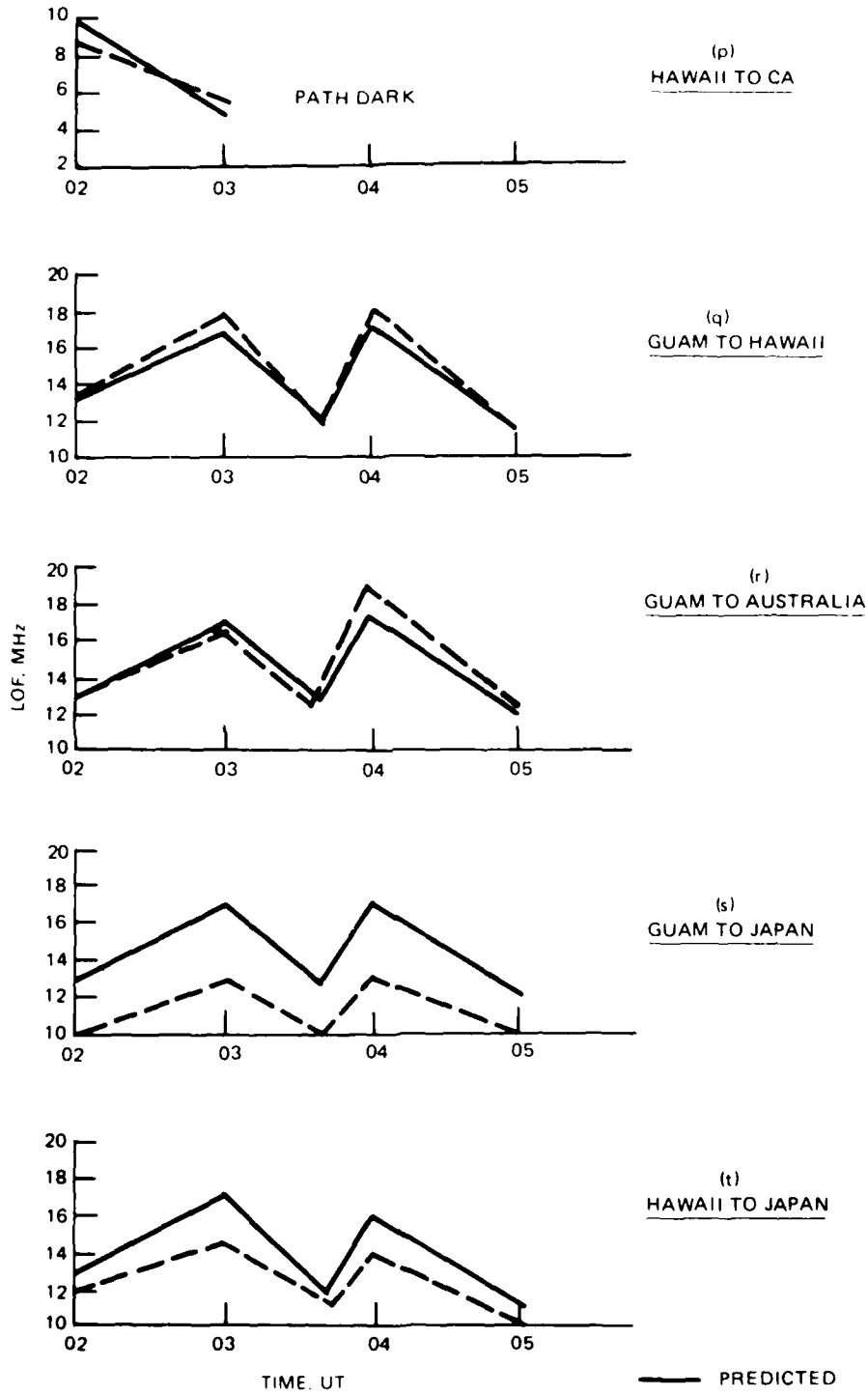

Figure 4. (Continued).

Table 4. Short-range HF LOF/X-ray flux algorithm tests, 803-km path.

Date	Time	ψ	F_X	Observed SWF LOF	Calculated SWF LUF	Error, MHz	Pre-event LOF
2 Jul 1971	1845	20.00	0.022	11.50	11.51	+0.01	5.95
7 Jul 1971	1507	62.906	0.0063	4.95	4.89	−0.06	3.675
7 Jul 1971	1603	53.598	0.0089	6.35	6.53	+0.18	4.75
7 Jul 1971	1925	15.0	0.0028	6.95	7.02	+0.07	5.75
7 Jul 1971	1947	12.192	0.0053	8.30	8.31	+0.01	5.75
10 Jul 1971	1546	54.675	0.013	7.15	7.01	−0.14	3.875
12 Sep 1971	1624	61.125	0.044	8.70	8.31	−0.39	4.15
12 Nov 1971	1833	65.93	0.02	6.55	6.01	−0.54	4.75
20 Nov 1971	2049	56.454	0.018	7.15	7.35	+0.20	3.575

3.3.3 Complete Algorithm Test

A final test of the SIDGRID model was performed in an SWF event, for which oblique sounder data on both the (long-range) Hawaii-to-La Posta and (short-range) Davis-to-La Posta paths were available. The event chosen was an M4 X-ray event that peaked at 00 UT on 10 November 1971. The Davis-to-La Posta path was very near darkness, and the path LOF had already dropped to 2 MHz just prior to the event. It would be interesting to see whether the new short-range algorithm would show this, along with the rise of the LOF, at the SWF peak. Figure 5 shows excellent agreement between SIDGRID model predictions and observed oblique sounder information for this event.

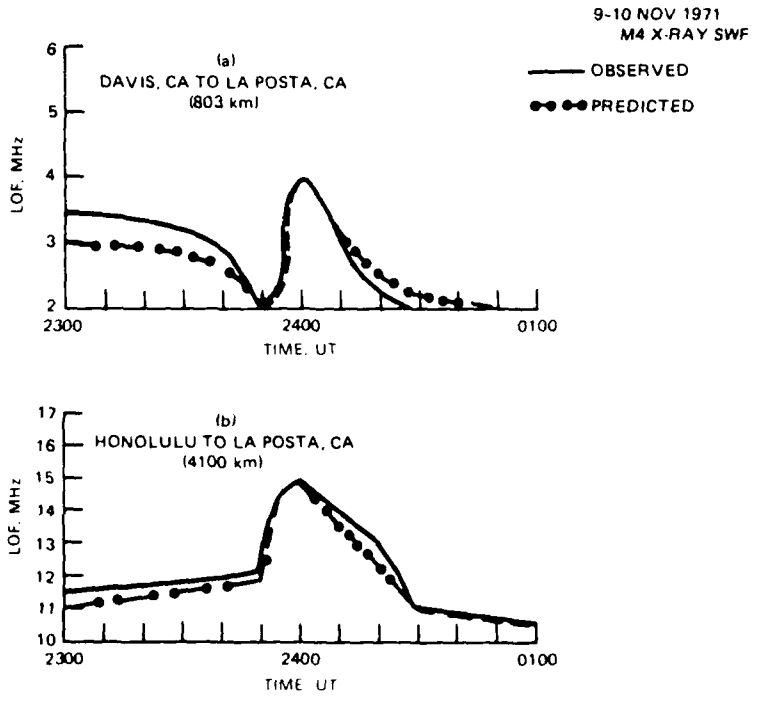

Figure 5. Two-path comparison of revised SIDGRID.

4.0 SUMMARY AND CONCLUSIONS

1. The NOSC solar X-ray/HF LOF algorithms provide an accurate assessment of the change in HF LOF for solar X-ray bursts greater than 1×10^{-3} erg/cm^2 · s and are valid over the entire sunlit hemisphere. The SIDGRID model has the ability to display the disturbed LUF for any path on the geographical sunlit hemisphere at any date and time. If the model is run with a continuous date/time clock, the only required input variable is 1–8-Å X-ray flux. Figure 6 shows the SIDGRID model display for an X-ray flare starting at 1600 UT and peaking at 1615 UT. The display shows the circuit blacked out from about 1610 UT to 1700 UT.

```
 1 MAR 1987  ■■■■■
10.7 CM FLUX = 73    SUNSPOT NUMBER = 12
X-RAY FLUX = 0.15000
MAGNETIC INDEX = 2.0
XMTR: WA      40.00N  75.00W              RCVR: SD      32.73N 117.17W
ANT: 25 (OMNI DIR)                      ANT: 25 (OMNI DIR)
BEARING (TO SD    ) = 271.4 DEG         BEARING (TO WA    ) = 65.6 DEG
RANGE = 3825 KM     POWER: 1000. W

FLARE START: 1600Z   FLARE PEAK: 1615Z
```

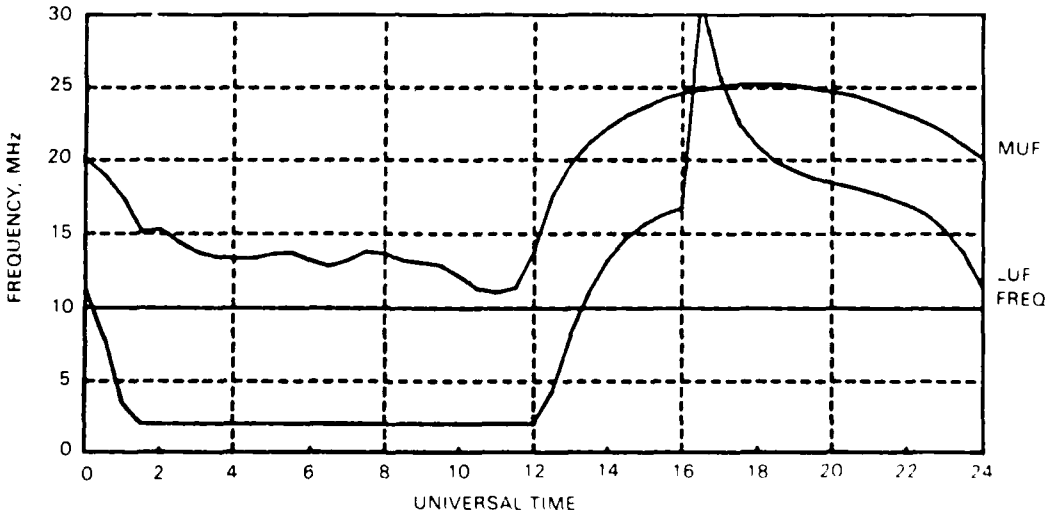

Figure 6. SIDGRID model display.

2. The SIDGRID models HF LUF over a transmission path based on the following range-dependent parameters:

Short-range $\leq$ 1500 km

Long-range > 1500 km.

Accuracy of the long-range algorithm was determined by comparing SIDGRID predictions to 198 observed sounder data points. Results from these tests indicate that the mean prediction error was 0.24 MHz and the error between predicted and observed data was negligible in 29% of the tests. The probability that the prediction error was less than or equal to $\pm$1.0 MHz was 83% and the probability of error less than +2.0 MHz was 95%.

Accuracy of the short-range algorithm is shown in table 4. Nine events were tested; the calculated SWF/LUF differed from the observed SWF over a range of −0.54 MHz to +0.20 MHz. The nominal accuracy specification for the short-range algorithm is ±0.5 MHz for HF transmission paths of less than 1500 km. For both algorithms, the accuracy of the computed HF LUF improves as the solar event size and duration increase.

The sudden ionospheric disturbance FORTRAN computer subroutine called DLOF is listed in Appendix C, and the BASIC subroutine is listed in Appendix D.

3. The SIDGRID model does not include a means to adjust the resultant LUFs for system parameters such as transmitted power, antenna gains, required signal-to-noise ratio, and background radio noise. Under the full impact of an SWF, the main contribution to the LUF is the D-region absorption. However, as the D-region begins to recover from the effects of the SWF, the transition to quiet time LUF prediction would be smoother if methods were developed to include these effects.

4. The SIDGRID model is strictly a LUF prediction model. It does not calculate the D-region absorption resulting from an SWF. Such a model is desirable so that the decrease in available signal strength between the LUF and MUF resulting from an SWF can be determined.

5. The SIDGRID model is a two-range model (short range $\leq$ 1500 km, long range $>$ 1500 km). An attempt should be made to keep the model continuous as a function of range.

5.0 REFERENCES

1. Naval Ocean Systems Center TR 186, MINIMUF-3: A Simplified HF MUF Prediction Algorithm, by R. B. Rose, J. N. Martin, and P. H. Levine, 1 Feb 1978.
2. NOSC TD 201, MINIMUF-3.5, Improved Version of MINIMUF-3, A Simplified HF MUF Prediction Algorithm, by R. B. Rose and J. N. Martin, 26 Oct 1978.
3. NOSC TR 1121, MINIMUF-85: An Improved HF MUF Prediction Algorithm, by D. B. Sailors, R. A. Sprague, and W. H. Rix, 19 Jul 1986.
4. Landmark, B., "The Ionosphere," paper presented at the NATO AGARD Lecture Series XXIX in Leicester, UK, 30 Jun to 5 Jul 1968.
5. Naval Electronics Laboratory Center TR 1782, HF Propagation Degradation During Ionospheric Storms, by R. B. Rose, 24 Aug 1971.
6. NELC TR 1774, System Performance Degradation Due to Varying Solar Emission Activity: SOLRAD Applications Study, Task II, by R. B. Rose, D. G. Morfitt, and M. P. Bleiweiss, 28 June 1971.
7. Naval Weapons Center TP 885, Observations of the Effects of Solar X-ray Radiation on HF Ionospheric Propagation, by B. E. Erickson, Sr., and V. F. Hildebrand, Nov 1969.
8. NWC TP 4976, Short-wave Frequency Degradation, by R. B. Rose, Sep 1970.
9. NELC TR 1938, Sudden Ionospheric Disturbance Grid, by R. B. Rose, J. R. Hill, and M. P. Bleiweiss, 1 Dec 1974.
10. NWC TP 4911, Solar Influences in HF Absorptions and the Resulting Hawaii to California Lowest Observed Frequency, by M. P. Bleiweiss, May 1970.
11. NELC TR 1851, A Prediction Scheme for the Lowest Observed Frequency (LOF) of the Guam-North West Cape HF Propagation Path and Eight Other Pacific Paths, by M. P. Bleiweiss, 6 Dec 1972.

APPENDIX A:
THEORETICAL BASIS

It is appropriate to look briefly at why the simple logarithm used to produce the SIDGRID works as well as it does. In references 10 and 11, it was determined that the undisturbed LUF is approximated by:

$$\text{LUF} = (\text{Constant})\,(\cos\chi)^{1/4}\ ,$$

where Constant = a function of D-region nondeviative absorption (A) plus transmitted power, system signal-to-noise ratio, launch angle, and antenna patterns.

In reference 10, it also was stated that the absorption (A) could be expressed by:

$$A \propto \frac{N_{(e)}}{f^2}$$

where

$N_{(e)}$ = electron density of the D-region
f = frequency of operation.

The D-region electron density can be defined as consisting of:

$$N^2_{(e)} = N^2_{(e)X} + N^2_{(e)UV}$$

where

$N_{(e)X}$ = electron density due to X-ray emission
$N_{(e)UV}$ = electron density due to ultraviolet Lyman Alpha (1216 – Å) emission.

$N_{(e)UV}$ remains essentially constant during quiet and disturbed solar conditions. $N_{(e)X}$ is a secondary contributor to absorption during undisturbed periods and becomes the primary contributor during disturbed periods. The SIDGRID algorithm was empirically developed on the basis of observed changes in X-ray emission and HF LOF. Because this relationship was established for the cases in which solar X-ray emissions are the principal cause of HF absorption, the accuracy of the algorithm should increase proportionally to the size of the X ray burst. In other words, the SIDGRID model is predicated on the expression:

$$\text{LUF} \propto (\text{Absorp}_{\text{X ray}}) \cdot (\cos\chi)^{1/4}\ .$$

As the magnitude of the input X ray emissions decreases, the HF system parameters increase in importance, complicating the constant calculation, and for the undisturbed case the HF LOF is expressed by:

$$\text{LUF} \propto (\text{HF system path parameters} + \text{Absorp}_{(UV)}) \cdot (\cos\chi)^{1/4}$$

Therefore, for extremely low levels of X ray emission, it can be expected that the accuracy of the SIDGRID model will diminish somewhat.

APPENDIX B:
TEST OF DOUBLE SWF ON 2 AUGUST 1972

Figure B-1 shows a composite of the HF propagation between Hawaii and Guam for the 24-hour period of 2-3 August 1972, the 1-8 Å X ray bursts that caused the two SWFs and (shaded area) the predicted SWF derived from the SIDGRID model. Time resolution is: one line equals a 10-minute average of the data. Signal amplitude is 25 dB above the receiver threshold.

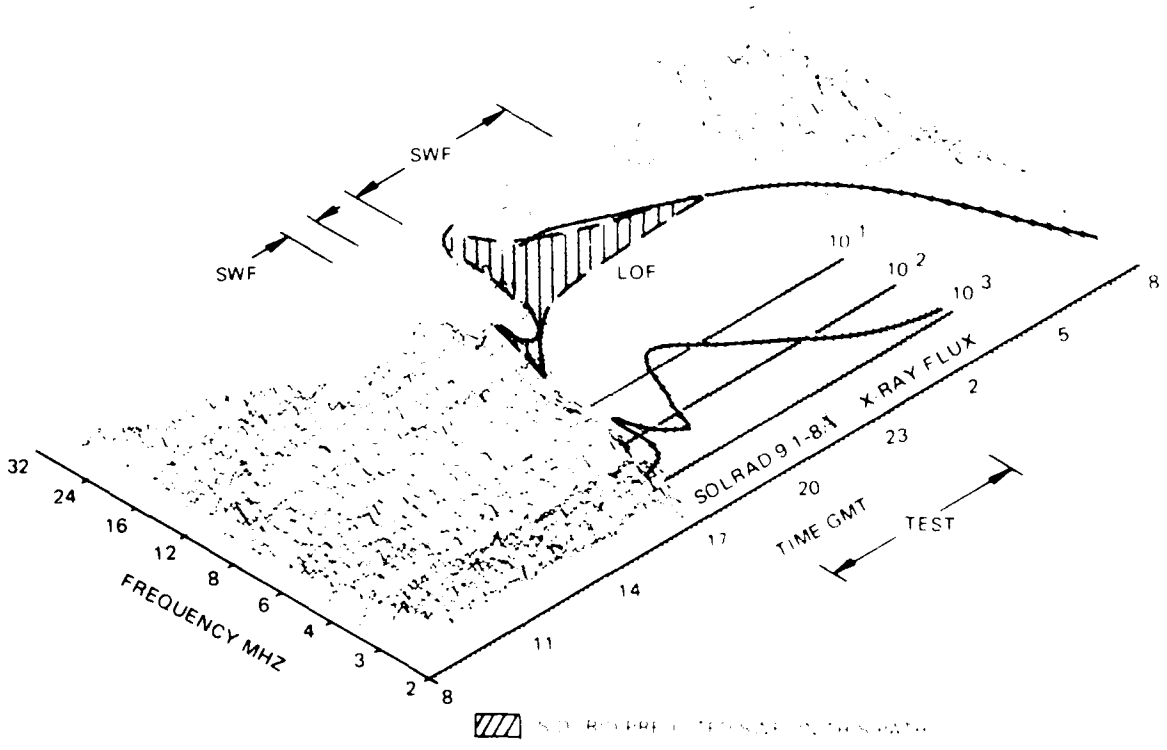

Figure B-1. 24-hour propagation characteristics, Guam to Hawaii 2-3 August 1972. Time resolution: 1 line – 10 min average. Signal amplitude: [illegible] 25 dB above receiver threshold.

APPENDIX C:
DLOF — FORTRAN SUDDEN IONOSPHERIC DISTURBANCE SUBROUTINE

```
      subroutine dlof ( tlat, tlon, rlat, rlon, xflux, cpnt, lof )
cp
c      subroutine dlof
c
c        call dlof(tlat,tlon,rlat,rlon,xflux,cpnt,lof)
c
c        this routine computes the luf for solar disturbed conditions (i.e.
c        xray flux > 1.83e-3.  tlat/tlon & rlat/rlon are the end point
c        coordinates in radians.  xflux is the current xray flux. cpnt is an
c        eight element array containing the path length and coordinates of
c        control points along the path (see subroutine path for complete
c        description).  this routine returns lof which is the luf in mhz.
c        this routine assumes west longitudes.
c
c        subroutines and functions used:  minpt
c                                         newton
c
c        common blocks:  sun
cz
      real          cpnt(8), lof
c
      common        /sun/     slat, slon
c
      lof = 0.5
      call minpt( rlat, rlon, cpnt, clat, clon, chi )
      dist = cpnt(1)*6371.0
      if ( chi .gt. 1.57 )  go to 100
      flux = xflux
c
      if ( dist .lt. 3500.0 )  go to 11
      call newton( chi, flux, lof )
      go to 100
11    x = sqrt(  (  flux*cos( chi )**3 )/1.03856e-6 )
20    lof = sqrt( x )
      theta = ( dist/6371.0 )*0.5
      alfa = ( cos( theta ) - 0.96224 )/sin( theta )
      alfa = atan( alfa )
      alfa = acos ( 0.9891*cos( alfa ) )
      lof = lof*sqrt( 0.5368/sin( alfa ) )
100   continue
      lof = amin1( amax1( lof, 0.5 ) , 50.0 )
      return
      end
```

APPENDIX D:
SIDGRID — BASIC SUDDEN IONOSPHERIC DISTURBANCE SUBROUTINE

```
4750 SUB Sidgrid
4760    A=S0
4770    B=S1
4780    C=Z3
4790    D=Z4
4800    CALL Geraz
4810    C7=R
4820    C=Z5
4830    D=Z6
4840    CALL Geraz
4850    C7=C7 MIN R
4860    IF C7<P0 THEN 4890
4870    L=2
4880    GO TO 5320
4890    FOR I=1 TO 9
4900       C=Z0(2*I+2)
4910       IF C=-999 THEN 4960
4920       D=Z0(2*I+3)
4930       CALL Geraz
4940       C7=C7 MIN R
4950    NEXT I
4960    C7=COS(C7)
4970    D=Z0(1)*R2
4980    IF D=>3500 THEN 5070
4990    X=SQR(SQR(F4*C7^3-1.03856E-6))
5000    T=D/12742
5010    A=ATN((COS(T)-0.96224)/SIN(T))
5020    A=0.9891*COS(A)
5030    A=A MAX -1 MIN 1
5040    A=ACS(A)
5050    L=X*SQR(0.5368/SIN(A))
5060    GO TO 5310
5070    B=1-C7^2
5080    X0=(F4/0.1038+150)/(10+B)
```

```
5090    C=1.0E-4
5100    X=X0
5110    E=X
5120    CALL Newton
5130    F=100*C
5140    FOR I=1 TO 20
5150      IF G=0 THEN 5300
5160      IF H=0 THEN 5290
5170      X1=G/H
5180      X=X-X1
5190      E=X
5200      CALL Newton
5210      E=C
5220      R=ABS(X)
5230      IF R<=1 THEN 5250
5240      E=E*R
5250      IF ABS(X1)>E THEN 5270
5260      IF ABS(G)<=F THEN 5300
5270    NEXT I
5280    GO TO 5300
5290    X=32
5300    L=X
5310    CALL Adjluf
5320 END SUB
5330 SUB Newton
5340    P=(1+B/10)*E
5350    Q=0.849*(P-15.6)
5360    Q=Q-INT(Q/P1)*P1
5370    G=0.01038*(P-15)-0.003*SIN(Q)
5380    G=G-F4
5390    H=(0.01038-0.0025473*COS(Q))*P.E
5400 END SUB
```

END

DATE

FILMED

DTIC

4/88